Bioconjugate Chemistry

pubs.acs.org/bc Article

Hydrophobic Cargo Encapsulation into Virus Protein Cages by Self-Assembly in an Aprotic Organic Solvent

Amberly Xie, Irina Tsvetkova, Yang Liu, Xingchen Ye, Priyadarshine Hewavitharanage, Bogdan Dragnea,* and Ruben D. Cadena-Nava*

Cite This: *Bioconjugate Chem.* 2021, 32, 2366−2376 Read Online

ACCESS | Metrics & More | Article Recommendations | Supporting Information

ABSTRACT: While extensive studies of virus capsid assembly in environments mimicking *in vivo* conditions have led to an understanding of the thermodynamic driving forces at work, applying this knowledge to virus assembly in other solvents than aqueous buffers has not been attempted yet. In this study, Brome mosaic virus (BMV) capsid proteins were shown to preserve their self-assembly abilities in an aprotic polar solvent, dimethyl sulfoxide (DMSO). This facilitated protein cage encapsulation of nanoparticles and dye molecules that favor organic solvents, such as β-$NaYF_4$-based upconversion nanoparticles and BODIPY dye. Assembly was found to be robust relative to a surprisingly broad range of DMSO concentrations. Cargos with poor initial stability in aqueous solutions were readily encapsulated at high DMSO concentrations and then transferred to aqueous solvents, where they remained stable and preserved their function for months.

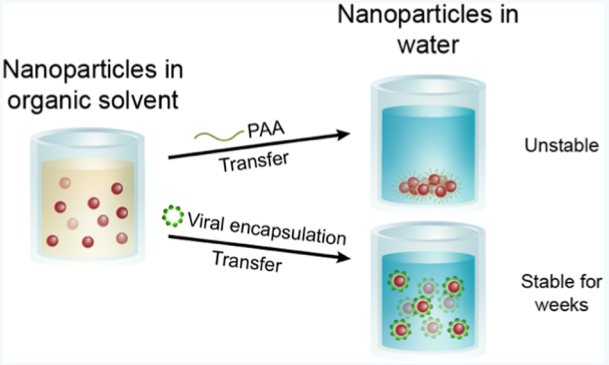

INTRODUCTION

Hybrid biotic−abiotic nanomaterials are a promising venue for materials with advanced synthetic control and enhanced physical and chemical characteristics.[1] For instance, superior optical properties, including luminescence and absorption, can be leveraged in manufacturing biocompatible nanoscopic sensors or deep subwavelength light emitters for nonintrusive optical control.[2] Such hybrid nanoparticles could be useful in influencing biological processes important for nanomedicine and environmental bioremediation applications.[3,4] One abiotic component of interest that has captured the attention of the scientific community over the past few years is the upconversion nanoparticle (UCNP).[5−8] UCNPs absorb low-energy infrared light and re-emit higher-energy visible light, which presents a wide range of potential applications in imaging, nanomedicine,[9] photovoltaics,[10] and more. UCNPs hold several advantages over traditional fluorescent probes: higher signal-to-noise ratios, owing to lack of background fluorescence, and less photodamage due to the use of low-energy near-infrared (NIR) light, which is weakly absorbed by tissues.[11] However, for this example and several other instances of luminescent probes with desirable photonic properties, potential biological applications have been hampered by the instability of abiotic components in aqueous media since many of them are more stable in organic solvents,[12] while biological processes in most cases are negatively affected by such solvents.[13]

One commonly used organic solvent in biological and medical applications is dimethyl sulfoxide (DMSO).[14] DMSO is an aprotic polar solvent that dissolves both polar and nonpolar compounds, is water-miscible in all proportions, and hydrogen bonds with water but not with itself. Water−DMSO mixtures have physicochemical properties, including viscosity, thermal and electrical conductivity, and colligative properties that depend nonlinearly on proportions.[15,16] DMSO has been routinely used with good results for the preservation of cells[17,18] and tissues,[19] and for the dissolution of chemotherapeutic agents,[20] fluorescent dye molecules,[21] quantum dots,[22] carbon nanotubes,[23] metallic nanoparticles,[24] and rare earth materials, such as UCNPs.[11] In DMSO−water solutions, the water radial distribution function retains the characteristic tetrahedral ordering of water−water hydrogen bonds even for highly concentrated DMSO solutions.[25] However, DMSO is known to perturb protein folding and dynamics.[26] The observed effects include protein compaction and changes in enzyme-substrate binding equilibrium.[27] At the cellular level, neuronal damage was observed in the presence of DMSO even at relatively low DMSO concentrations (0.5% mL/kg body

Received: August 25, 2021
Revised: October 14, 2021
Published: November 3, 2021

https://doi.org/10.1021/acs.bioconjchem.1c00420
Bioconjugate Chem. 2021, 32, 2366−2376

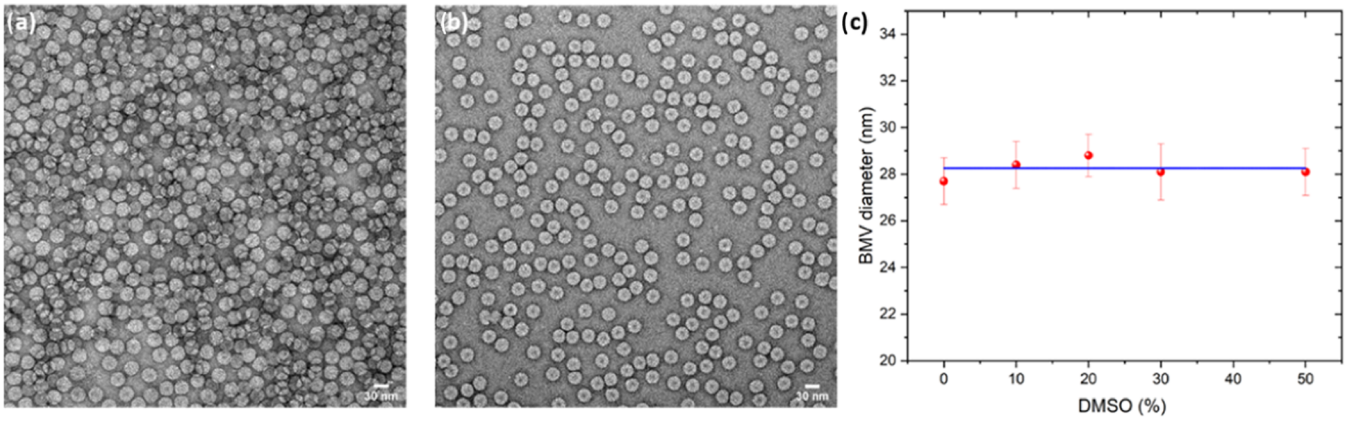

Figure 1. TEM micrographs of BMV (~.05 mg/mL) incubated for 48 h in (a) 0% DMSO and (b) 50% DMSO. (c) Average diameter measured by TEM at different concentrations of DMSO. The blue line shows an average diameter of 28.3 ± 0.2 nm over all concentration ranges; red bars are standard deviation.

weight).[28,29] Taken together, these results indicate a broad impact spectrum of DMSO on biomolecular function, ranging from innocuous to perturbative, on a case-by-case basis.

Self-assembling viruses are excellent encapsulators offering large payloads, chemical addressability, reconfigurability, and reduced size polydispersity.[30−34] While many virus shells have been shown to assemble *in vitro* around cognate nucleic acids or noncognate cargo, up to now, it was unknown whether the addition of DMSO to the assembly buffers would perturb the assembly process. However, this knowledge is desirable for molecules and nanomaterials that require high concentrations of DMSO to be dissolved. For instance, here, we explore encapsulation of poorly water-soluble cargo inside virus-like particles (VLPs) in DMSO solutions, followed by the transfer of the VLPs into DMSO-free physiological buffers, thus making them available for biomedical applications. Such VLPs have structurally similar cages with that of the wild type (wt) virus and presumably preserve some of its appealing attributes. In place of the genomic material, they could carry a variety of different nanoparticles or molecular cargo, the range of which this work promises to extend. Such VLPs will be useful in the development of vaccines, as nanocarriers of therapeutic molecules, or for imaging and sensors in disease detection.[35]

Usually, *in vitro* synthesis of VLPs is carried out in aqueous media.[36] To the best of our knowledge, self-assembly of VLPs in DMSO-containing solutions has never been studied. Presumably, the known DMSO ability to inactivate viruses and denature certain proteins[26,37,38] has dampened the enthusiasm for such explorations. However, the capsids of many icosahedral plant viruses are stabilized by the hydrophobic effect, and previous computations suggest that the water hydrogen-bonding network should be minimally affected by mixing with DMSO.[25] Moreover, plant viruses have proven to be stable and resistant to organic solvents up to 50% (v/v) during their purification process,[39] as well as for short periods of time in up to 20% DMSO during chemical functionalization of the capsid with hydrophobic molecules,[40−44] suggesting the possible persistence of native interactions in DMSO/water solutions.

Here, we report on experimentally testing the hypothesis that self-assembly of viral capsids in DMSO solutions could occur. If confirmed, this could expand the potential uses of VLPs as transfer vehicles of poorly soluble nanocompounds between organic and aqueous media. Specifically, brome mosaic virus (BMV) capsid proteins (CPs) were co-assembled with UCNPs and BODIPY (Bdpy) fluorescent molecules. Not only was the formation of VLPs in up to 30% (v/v) of DMSO successful, but the viral protein shell also dramatically increased the lifetime of cargo solubility when transferred to aqueous media and consequently provided a way to preserve cargo optical properties for much longer than previously possible. Though previous experiments have developed water-soluble UCNPs through modifying the surface with hydrophilic ligands[45,46] and the use of metal−organic frameworks,[47] the engineering of UCNPs exhibiting long-term stability in aqueous solutions remained largely unexplored. Thus, the method presented here provides advantages in facile encapsulation and transfer of UCNPs to aqueous media, obtaining colloidally stable nanoparticles, and allowing for easy chemical and biochemical modifications to the VLP-UCNPs through the protein shell.

The work demonstrates that it is indeed possible to transfer and preserve cargo functions from organic to aqueous media by encapsulation in a virus-like cage via virus coat protein co-assembly, opening the door to a host of possible novel biomedical studies and applications.

RESULTS AND DISCUSSION

Stability of wtBMV in DMSO. As a first step, the stability of wtBMV in DMSO solutions was studied. After 48 h of incubation at various concentrations of DMSO, virus morphology was characterized by transmission electron microscopy (TEM) and dynamic light scattering (DLS). Figure 1 shows TEM images of wtBMV in virus storage buffer (SAMA) without DMSO and with 50% DMSO. wtBMV at concentrations of 10, 20, and 30% DMSO are shown in Figure S1. At these concentrations, the virus remained stable, with no morphological changes with respect to wtBMV in SAMA. The average diameter of BMV at these concentrations of DMSO was found to be 28.3 ± 0.9 nm, which is very similar to that of wtBMV (27.6 ± 0.9 nm) without DMSO (Figures 1c and S1). However, wtBMV was not observed at concentrations greater than ~80% DMSO, potentially due to DMSO significantly increasing the apparent pH at these concentrations.[48]

Empty BMV Capsid Assembly in DMSO Solutions. It is well known that BMV CPs can self-assemble spontaneously at high ionic strength and low pH into empty capsids (EC).[49−52] The capsid is stabilized by intercapsomeric hydrophobic

https://doi.org/10.1021/acs.bioconjchem.1c00420
Bioconjugate Chem. 2021, 32, 2366−2376

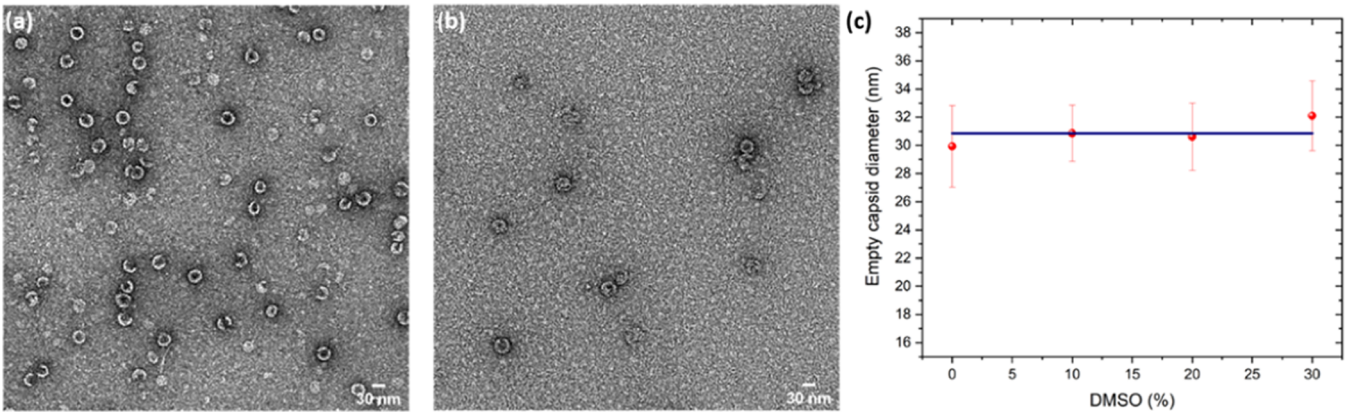

Figure 2. TEM of empty capsids assembled at (a) 0% DMSO and (b) 30% DMSO at low ionic strength (0.005 M $MgCl_2$). (c) Average diameter of ECs assembled in DMSO solutions measured by TEM. The blue line shows the average diameter (30.8 ± 0.5 nm) over all concentration ranges; red bars show the standard deviation.

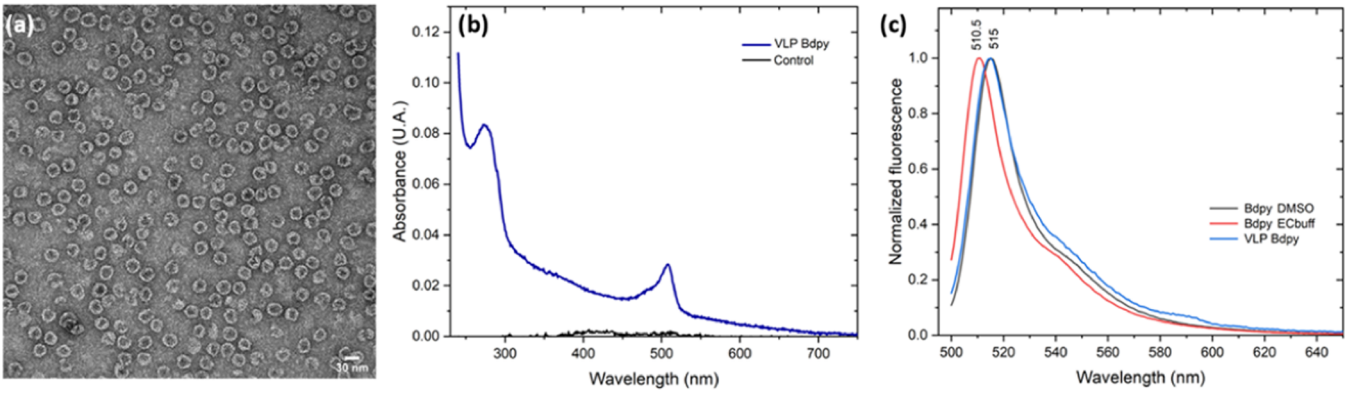

Figure 3. (a) TEM image of VLP-Bdpy assembled in 30% DMSO at an initial molar ratio of 10 Bdpy:1 CP (b) absorbance and (c) fluorescence spectrum of VLP-Bdpy in EC buffer. The fluorescence spectrum was taken with 490 nm excitation.

interactions. Since DMSO can hydrogen-bond with water but not with itself, the question is whether the hydrophobic effect is sufficient in concentrated DMSO solutions to drive assembly. Previous studies have shown that salts in DMSO solutions have lower solubility than in water.[53,54] Since it is known that BMV EC assembly can occur in acidic, low ionic strength (<100 mM NaCl),[49,55] EC assembly was conducted at relatively low ionic strength buffers (50 mM NaOAc, 5 mM $MgCl_2$) in the presence of DMSO. Assembly of empty capsids was studied *in vitro* at concentrations of 0, 10, 20, and 30% DMSO by volume. Above 30%, assembly efficiency was very low. In addition to EC formation, partial capsids and ribbons were observed. Figure 2 shows TEM micrographs of the assembled empty capsids in 0 and 30% DMSO (ECs assembled in 10 and 20% DMSO are shown in Figure S2). The average diameter of the assembled empty capsids at different concentrations of DMSO is similar to that of wtBMV and of ECs assembled at low pH in aqueous buffers, as shown in Figure 2c. Average EC diameters were 29.9 ± 2.9, 30.8 ± 2.0, 30.6 ± 2.4, and 33.4 ± 4.1 nm at 0, 10, 20, and 30% DMSO, respectively. Thus, a slight increase in the average diameter was observed at higher concentrations of DMSO. This can likely be attributed to DMSO interrupting CP−CP hydrophobic interactions[56] as well as slightly increasing solution pH.[48] BMV is known to exhibit a swelling structural transformation when the pH is increased above pH 6.[57] Intriguingly, empty capsids do not swell in aqueous buffers; when transferred to a neutral pH solution, they usually disassemble. These results demonstrate the ability of BMV CPs to self-assemble into empty capsids at concentrations of up to 30% DMSO, which suggests that the hydrophobic interactions which normally stabilize BMV capsids in physiological buffers are still at least partially at work in DMSO−water solutions.

To study theoretically the molecular interaction between DMSO and BMV CPs, molecular docking studies were performed. The most probable DMSO-BMV CP binding conformations were obtained by AutoDock Vina software (Figure S3a).[58] These conformations have affinity energies of −2.4 kcal/mol on the interior interface of the CP and −1.4 kcal/mol in the unstructured region of the N-terminus. DMSO was predicted to mostly bind close to random coil structures and did not have an affinity for the β barrel region, which is key for intercapsomeric interactions. These results qualitatively agree with other works, where the influence of DMSO on proteins was studied[59,60] and confirm that CP−CP interactions are not drastically affected by DMSO.

Self-Assembly of VLP-Bdpy in DMSO. We extended our newly acquired knowledge of EC assembly in DMSO to test if DMSO-solvated small organic dyes could be encapsulated by BMV CPs. In particular, a boron dipyrromethene dye derivative (Bdpy) was used as a model hydrophobic dye molecule. TEM analysis revealed the proper formation of VLPs (Figure 3a). VLP-Bdpys had an average diameter of 30 ± 1.2 nm as measured by TEM (Figure S4).

https://doi.org/10.1021/acs.bioconjchem.1c00420
Bioconjugate Chem. 2021, 32, 2366−2376

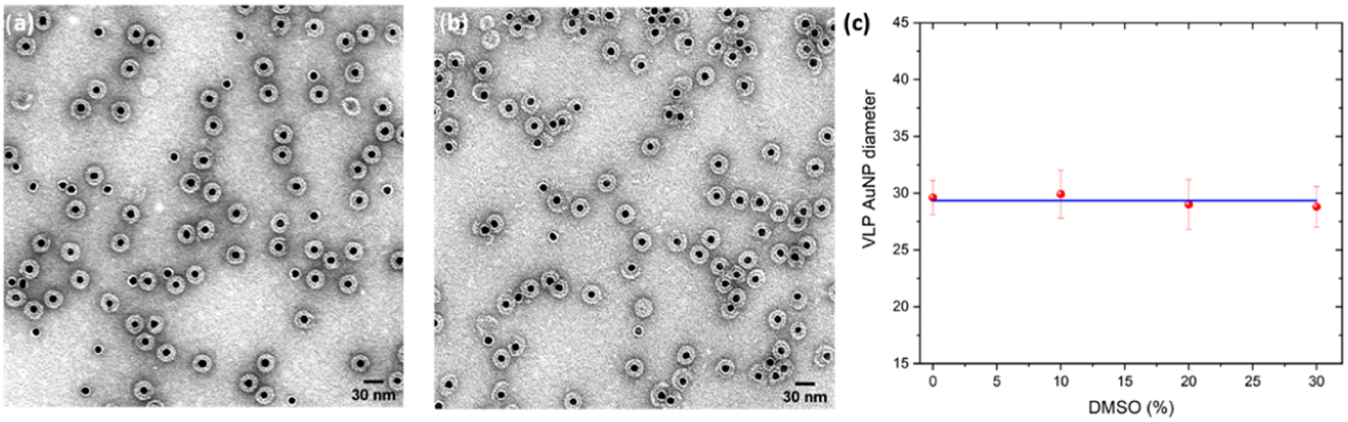

Figure 4. TEM images of VLP-AuNPs-12.3 assembled at (a) 0% and (b) 30% DMSO. Capsomeric organization is apparent in VLP shells in both cases. (c) Average VLP-AuNP-12.3 diameter measured by TEM at different concentrations of DMSO. The blue line shows an average diameter of 29.3 ± 0.2 nm, independent of DMSO concentration; red bars show standard deviation.

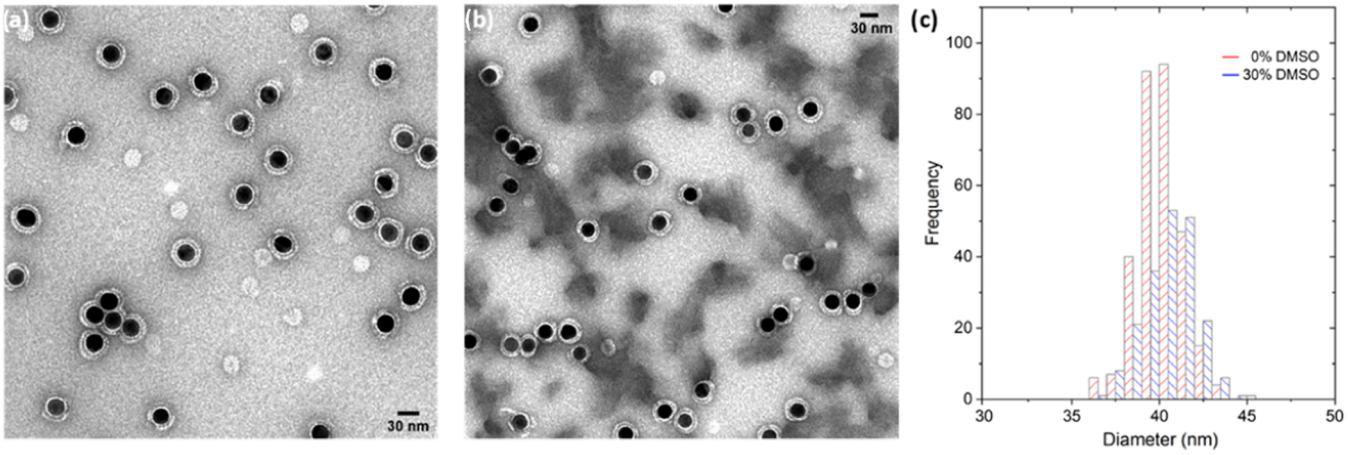

Figure 5. TEM images of VLP-AuNPs-25.8 assembled (a) without DMSO and (b) in 30% DMSO. Examples of protein shell defects are indicated by red arrows. (c) Size distributions by TEM of VLP-AuNPs-25.8 at 0% (red) and 30% DMSO (blue).

The absorbance spectrum of VLP-Bdpy is shown in Figure 3b. The major absorbance peaks for VLP-Bdpy were found at 280 and 508 nm, corresponding to BMV CPs and Bdpy absorbances, respectively. To ensure that the observed absorption signals were from capsid-associated and not free dye in solution, potential free Bdpy dyes were dialyzed against the EC buffer, and the solution in the dialysis bag was used for UV−vis absorption measurements ("Control" in Figure 3b). Practically zero absorption was observed, supporting the idea that the observed absorption in the VLP-Bdpy sample was due to encapsulated Bdpy dyes and not from free dyes in the solution. The UV/Vis absorption spectra for ECs and Bdpy were fitted via a multipeak procedure using a linear combination of pure substance spectra to determine the CP/Bdpy molar ratio (see Materials and Methods and Figure S5). From fitting the data in Figure 3b, we estimate ∼160 Bdpy dyes per VLP, which corresponds to roughly one Bdpy per CP.

Additionally, the fluorescence spectra from VLP-Bdpy show a peak at 515 nm for both free dye in DMSO and for VLP-Bdpy in EC buffer (Figure 3c). The peak intensity wavelength of free Bdpy fluorescence depends on DMSO concentration, with the Bdpy major peak being at 510.5 nm in 0% DMSO (Figure S6a). The same peak wavelength for free Bdpy in DMSO and VLP-Bdpy (Figure 3c) is likely due to the fact that DMSO has a similar refractive index to the CP[15,61] and suggests that in VLP-Bdpy, the dye is mostly surrounded by a medium different from water, *i.e.*, it must be in tight contact with the protein. We note that trapping of hydrophobic molecules in viral capsids has been demonstrated previously,[62,63] but it has not been accomplished until now by co-assembly of CP and dyes in a DMSO solution.

The most probable Bdpy-BMV CP binding site was investigated through molecular docking simulations. The highest docking scores of Bdpy with BMV CP are shown in Figure S3b. The simulations predict that Bdpy binds strongly at the capsid−capsid interface (binding energy ∼6 kcal/mol). Strong binding is supported by the observation that Bdpy remains bound to the CP after mixing with and dialysis against disassembly buffer (Figure S6b). From simulations, it appears that multiple Bdpy dyes could bind to the CP. This seems inconsistent with our estimates of ∼1 Bdpy per CP from UV−vis absorption spectrometry. However, since simulations were done on free protein while the experiments were done on full capsids, this difference is not surprising. Note that if there were as many Bdpy dyes between CPs as the simulations suggest, intercapsomeric interactions would have likely been weakened to the point of preventing VLP formation. In support of this, the observed increase in the size of the VLP-Bdpy compared to ECs (Figure S4c) suggests a tendency of the Bdpy dye to decrease the local curvature when bound and therefore strain

https://doi.org/10.1021/acs.bioconjchem.1c00420
Bioconjugate Chem. 2021, 32, 2366−2376

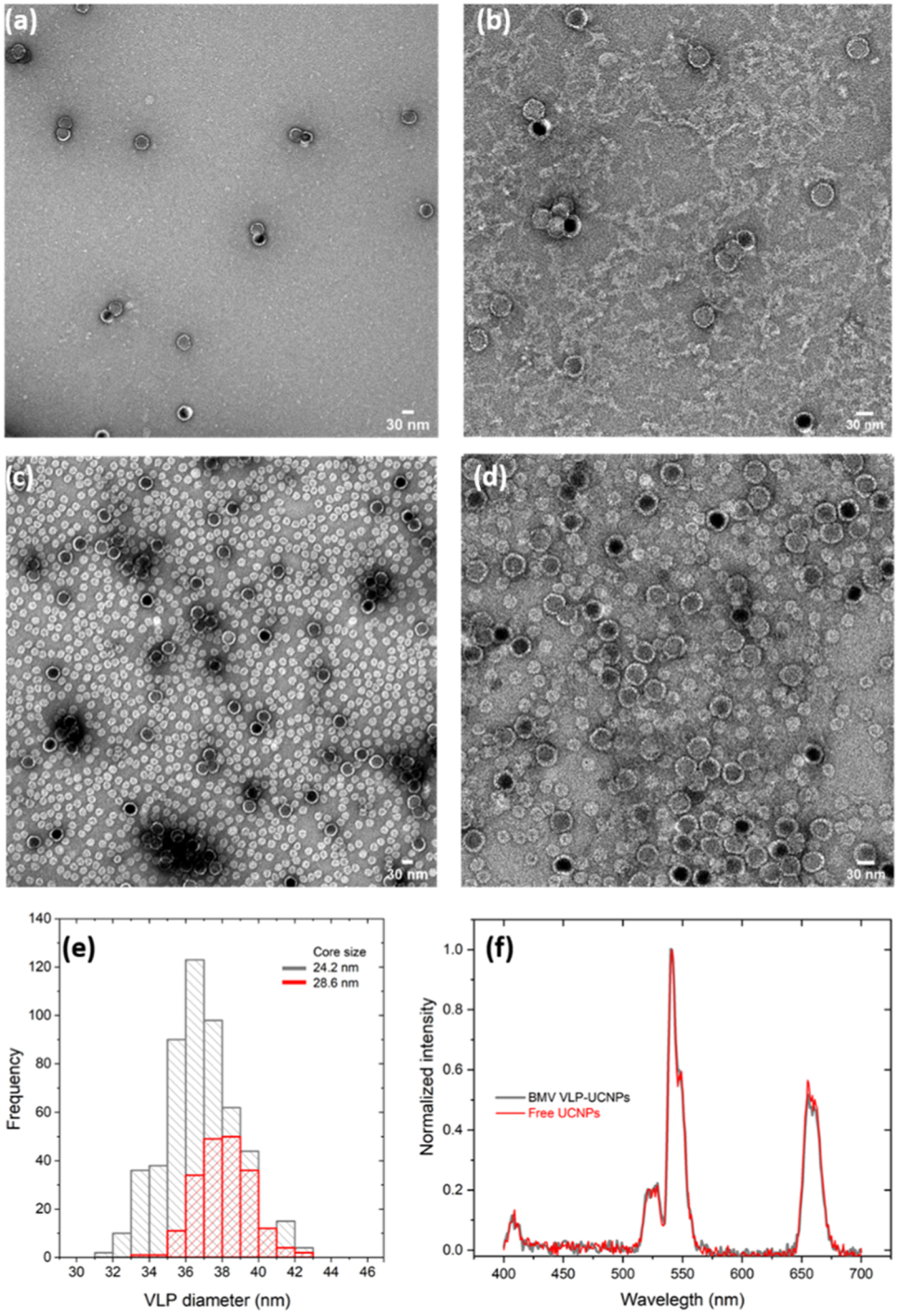

Figure 6. (a) TEM image of VLP-UCNPs-24.2 (arrow indicates protein shell defects). (b) The same sample as (a) after 8 months in storage at 4 °C. (c) VLP-UCNPs-28.6 after assembly and (d) after 4 months, stored at 4 °C. (e) Size distributions by TEM of UCNP-VLPs, with average diameters of 36.7 ± 2.2 nm (gray) and 38.1 ± 1.8 nm (red) for 24.2 and 28.6 nm diameter UCNPs, respectively. (f) Luminescence spectra obtained with an excitation wavelength of 980 nm, normalized against the 540 nm peak, comparing the VLP-UCNPs-24.2 dispersed in aqueous media (black) with free UCNP-24.2 dispersed in 100% DMSO (red).

the shell. Similar results have been found with the intercalation of heteroaryldihydropyrimidine at the dimer interfaces of HBV capsid assembly.[64,65]

Self-Assembly of BMV VLP-AuNPs in DMSO. Since the presence of DMSO was shown to negligibly interfere with CP−CP interactions, the next step was to study if DMSO would affect assembly interactions leading to cargo encapsulation. Specifically, the main driving forces in BMV are the electrostatic interactions between the positively charged N-terminus of the CP and a negatively charged cargo. To this end, anionic nanoparticle−CP co-assembly assays were carried out at a concentration of 30% DMSO. To study the ability of BMV CPs to encapsulate nanoparticles in the presence of DMSO, 12.3 ± 0.9 nm diameter spherical gold nanoparticles (AuNP-12.3, Figure S7) functionalized with an anionic polymer (PEG) were used. Figure 4 shows TEM images of

https://doi.org/10.1021/acs.bioconjchem.1c00420
Bioconjugate Chem. 2021, 32, 2366−2376

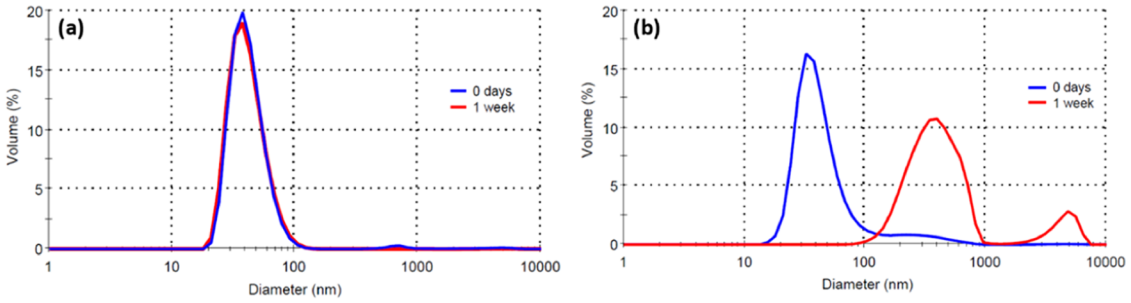

Figure 7. DLS measurements of (a) VLP-UCNPs-24.2 in SAMA buffer immediately after encapsulation and 1 week later. The most prominent peak at 42.4 nm remained constant 1 week after encapsulation. (b) Free PAA-coated UCNPs in SAMA buffer immediately after transfer into SAMA buffer and 1 week later.

the VLP-AuNPs-12.3 assembled at concentrations of 0 and 30% DMSO (assemblies at 10 and 20% DMSO, as shown in Figure S8). In all cases, VLP-AuNPs-12.3 had an average diameter close to 29.2 nm (Figure 4c). No structural differences were observed between the VLP-AuNPs-12.3 assembled with and without DMSO.

Assembly of BMV VLPs in DMSO solutions at all NP radii tested shows similar features to previous VLP-AuNP assembly studies in aqueous buffers. TEM images of VLPs obtained with 25.8 nm AuNPs (Figure S9) are shown in Figure 5. Structurally similar VLPs were obtained both with and without DMSO, with an average diameter of 40.2 ± 1.3 and 40.6 ± 1.5 nm, respectively (Figure 5c). In these cases, a few of the VLP protein shells contain defects, describable as breaks or packing defects in the protein shell (red arrows in Figure 5). Thus, the presence of these defects is likely due to the size of the nanoparticle core itself and not the presence of DMSO.

Self-Assembly of VLP-UCNPs in DMSO. The above CP−gold NP co-assembly assays confirmed that NP encapsulation can be carried out in DMSO solutions and that, structurally, the VLPs thus formed are not distinguishable from those previously obtained in assembly buffers. In this section, we turn our attention to a new cargo—UCNPs and their encapsulation into BMV VLPs as an approach to transfer and preserve them in a physiological buffer. To carry out this study, 24.2 nm diameter UCNPs coated with poly(acrylic acid) (PAA) were used (UCNP-24.2, Figure S10). A TEM image of the resulting VLPs is shown in Figure 6a. The resulting VLP-UCNPs-24.2 were found to have an average diameter of 36.3 ± 2.1 nm (gray distribution in Figure 6e). Subtracting the UCNP diameter from the measured average diameter and dividing by two yields a protein shell thickness of ∼6 nm, which is reasonably close to the BMV CP shell thickness of ∼5 nm,[66] supporting that CP has not been denatured upon coating the UCNP and that the observed protein coat has similarities to that of the BMV capsid. However, protein shell packing defects were observed on the surface of the VLP-UCNPs-24.2 (red arrows on Figure 6a), likely resulting from the larger size of the UCNP core (as discussed previously). The resulting VLPs were also somewhat heterogeneous, with some appearing slightly elongated. One possible cause for the observed shape deviations could be due to variations in UCNP morphology.

The ability of BMV CPs to encapsulate UCNPs in DMSO solutions extends to larger UCNPs as well. Figure 6c shows VLP-UCNPs-28.6 nm (Figure S11) immediately after assembly. Capsids lacking NP cores also formed, which likely resulted from the encapsulation of free PAA desorbed from UCNPs in solution. To remove free PAA, the sample was dialyzed against high pH (pH 7.2) assembly buffer (Figure S12). The average size of these VLPs was 38.1 ± 1.8 nm in diameter (red distribution in Figure 6e).

One question to be addressed is whether the optical emission properties of encapsulated UCNPs were affected by transferring them to aqueous buffer. Optical characterization of the VLP-UCNPs-24.2 was carried out by means of fluorescence spectroscopy. Figure 6f shows the luminescence spectra of free freshly prepared and encapsulated UCNP-24.2 in buffer. The spectra are nearly identical in the range of 400 to 700 nm, demonstrating that encapsulation and transfer did not affect the optical properties of UCNPs.

To test the stability of the VLP-UCNPs in aqueous media, VLP-UCNPs-24.2 were analyzed by TEM 8 months after encapsulation (Figure 6b). VLP-UCNPs-24.2 retained their morphological characteristics compared to the freshly synthesized VLPs, demonstrating remarkable long-term stability in aqueous solvents. Intriguingly, VLP-UCNPs-28.6 were also found to be stable despite visible shell packing defects. They showed identical morphology to the freshly assembled VLPs 4 months after assembly, as shown by TEM analysis (Figure 6d), once again demonstrating their impressive long-term stability in aqueous environments due to their protective protein shell.

The stability of free UCNPs and encapsulated UCNPs in aqueous buffer was compared using dynamic light scattering (DLS). Measurements from the same sample were taken right after mixing the UCNPs with aqueous virus storage buffer (SAMA) or right after encapsulation for the VLP-UCNPs-24.2 and 1 week later. The hydrodynamic radius of the VLP-UCNPs-24.2 remained constant after 1 week (Figure 7a), which can be attributed to stabilization by the capsid protein shell. While, at first, the free UCNPs appear stable in aqueous solvent, the main DLS peak shifts to a larger hydrodynamic radius in less than a week, demonstrating their limited stability in aqueous media despite the hydrophilic surface imparted by the PAA ligand (Figure 7b). These findings support the results obtained by TEM from freshly assembled and stored VLP-UCNPs (Figure 6).

Since the similarity of optical properties between freshly prepared PAA-coated UCNPs and UCNP-VLPs is striking, we have performed molecular docking simulations to understand the interplay between DMSO and PAA during nanoparticle encapsulation. Molecular docking was carried out with a short PAA (290 Daltons). Figure S3c shows the highest scoring binding conformations for the binding of PAA on the N-terminus of BMV CP with a corresponding affinity energy of −2.7 kcal/mol. PAA binds to positively charged regions of the N-terminus. Therefore, even though DMSO molecules could

https://doi.org/10.1021/acs.bioconjchem.1c00420
Bioconjugate Chem. 2021, 32, 2366−2376

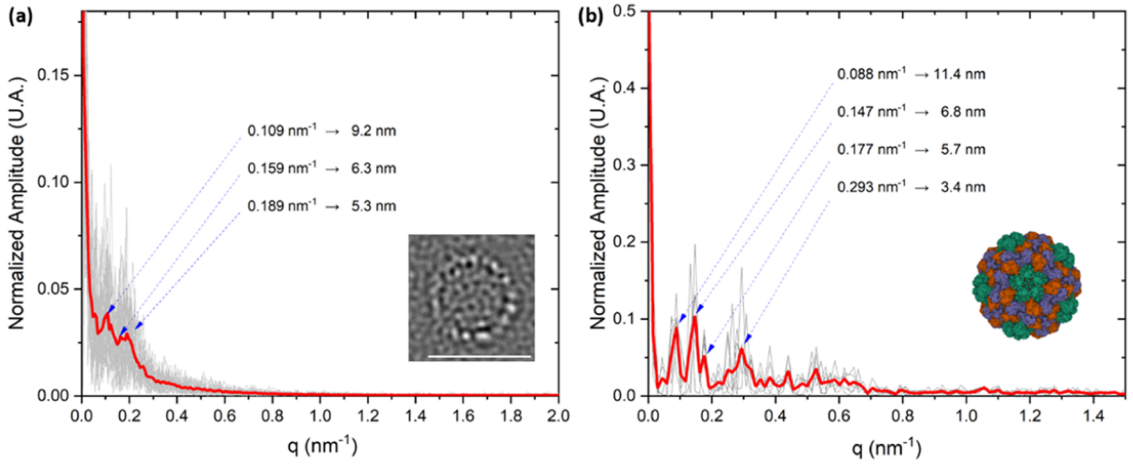

Figure 8. (a) Contour analysis of VLP-UCNPs-28.6 nm by fast Fourier transform (FFT). (b) Contour analysis of cryo-EM wtBMV (PDB 1JS9) using the 6-, 5-, and 2-fold projections, as well as one structure without symmetry. Red curves correspond to the average FFT.

interact with the N-terminal region of the CP, they will likely be displaced by PAA due to its higher affinity energy. This suggests that the mechanism underlying VLP-UCNP stability is capsid protein interactions retaining PAA and preventing NP coat degradation.

Capsomeric Order in VLP-UCNP Shells. To obtain more information on the capsomeric order in VLP-UCNP shells, rectangular strips of the VLP protein coats generated from TEM images were studied (Figure S13). A comparison of the spatial Fourier transforms between the VLPs and a BMV molecular model for different orientations and at 3.40 Å resolution[67] yielded a prominent peak doublet at ∼0.150 nm^{-1} (6.5 nm), which, by comparison with the molecular BMV capsid model, can be assigned to the capsomeric unit characteristic size (Figure 8). Thus, the VLP shell has at least a locally well-defined structure. However, assigning a triangulation number was not possible (see Supporting Information for further details).

CONCLUSIONS

Overall, this study demonstrates that the BMV VLP cargo encapsulation can occur directly in the organic solvent in which a cargo is stable, a process that enables transferring an insoluble cargo to an aqueous environment. This is possible because BMV CP−CP interactions are sufficiently preserved in DMSO/water solutions to promote assembly into capsid-like structures. Encapsulation of noncognate cargo by co-assembly with CP in DMSO/water solutions was demonstrated with hydrophobic Bdpy dyes and upconversion nanoparticles. Both cargoes were initially unstable in aqueous media, but they became stable after encapsulation in buffers containing up to 30% DMSO and could be subsequently transferred into DMSO-free buffers, where they remained stable for extended periods of time (months). Thus, BMV VLPs assembled in DMSO were shown to have the potential as nanocontainers for transporting hydrophobic cargo from aprotic polar organic solvents to aqueous solvents, ensuring the stability of the cargo in a physiological medium for extended periods of time. Such VLPs could open new possibilities in the medical field of diagnostic imaging.

MATERIALS AND METHODS

Nanoparticle Synthesis and Functionalization. *Gold Nanoparticles (AuNPs).* Citrate-coated gold nanoparticles with an average diameter of 12.3 nm were prepared following the Slot & Geuze method.[68] Functionalization of gold nanoparticles was performed by exchanging the initial citrate molecules with thiol-terminated poly(ethylene glycol) (TEG, ProChimia Surfaces, Poland). For 100 mL of the AuNP solution, 1 μL of TEG was added and allowed to stir overnight at room temperature. The functionalized gold nanoparticles particles were purified and concentrated by centrifugation. The resulting AuNP solution was characterized using TEM, and its concentration was obtained from UV−vis absorption spectroscopy.

Upconversion Nanoparticles (UCNPs). Upconversion nanoparticles were synthesized following previously described methods.[69] The native alkyl ligands were removed following a literature protocol,[70] resulting in electrostatically stabilized UCNPs that are highly soluble in DMSO. Next, UCNPs (nominal diameter: 25 nm) were functionalized with poly(acrylic acid) (PAA, 2000 MW, Sigma-Aldrich 323667-100G) by dropwise addition of 5 mL DMSO solution of UCNPs into a separate DMF solution of PAA (2 mg/mL). The resulting mixture was stirred for 1 h, after which 5 mL of toluene was added and followed by centrifugation at 6000 rpm for 2 min. Afterward, the UCNP precipitates were redispersed in 2 mL of DMF, to which 5 mL of toluene was added. Upon centrifugation at 6000 rpm for 2 min, the UCNP pellets were redispersed in DMSO for further characterization.

Brome Mosaic Virus (BMV) Capsid Protein Purification. BMV was purified from infected Atlantic barley (*Hordeum vulgare*) leaves,[71] and capsid proteins were purified as previously described.[36] BMV virions were disassembled by 24 h dialysis against disassembly buffer (0.5 M $CaCl_2$, 10 mM Tris, pH 7.6) at 4 °C and then by ultracentrifugation at 32 000 rpm for 30 min, at 4 °C in a Beckman type 70 TI rotor. The RNA pellet was discarded, with the liquid phase being kept. The sample was dialyzed against TKM buffer (1 M KCl, 10 mM Tris, $MgCl_2$, pH 7.4, 1 mM EDTA) and stored at 4 °C. The concentration and purity of the capsid proteins were measured by UV/Vis spectrophotometry. Protein solutions with 280/260 ratios greater than 1.5 were used for assembly.

https://doi.org/10.1021/acs.bioconjchem.1c00420
Bioconjugate Chem. 2021, 32, 2366−2376

SDS-PAGE was used to ascertain the integrity of the purified protein.

Empty Capsid (EC) Assembly. ECs assembly was based upon previous work from Pfeiffer,[49] with the modification of the assembling in the presence of 10, 20, and 30% DMSO by volume. BMV CPs protein (0.5 mg/mL) were dialyzed overnight against low ionic strength EC buffer (EC buffer: 50 mM NaOAc, 5 mM $MgCl_2$, pH 4.5).

VLP Assembly (Around AuNP and UCNP). VLPs were synthesized as reported previously[36] with slight modifications in buffers and protein to nanoparticle ratio. 260 BMV capsid proteins (CPs) were used per AuNP-12.3 and 870 CP for the encapsulation of AuNP-25.8, UCNP-24.2, and UCNP-28.6. For assembly of VLP-UCNP, we estimated the concentration of the synthesized nanoparticles according to Mackenzie et al.[72] to the concentration of UCNPs constant in the assemblies. Taking into account the calculated concentrations of the UCNPs, the assemblies were performed at 300:1 and 800:1 CPs to UCNP for the 24.2 and 28.6 nm nanoparticles, respectively. To find the best self-assembly conditions at high concentrations of DMSO, BMV CPs were self-assembled around 12.3 nm AuNPs at concentrations of 10, 20, and 30% DMSO by volume, with 30% yielding the best results. For VLP assembly, a mixture of nanoparticles, BMV CPs, and TKM buffer (1 M KCl, .01 M Tris, .005 M $MgCl_2$, pH 7.4) was adjusted to reach a final concentration of protein 0.4 mg/mL and 30% DMSO before dialysis and dialyzed against TNKM buffer (0.05 M Tris, 0.05 M NaCl, 0.01 M KCl, 0.005 M $MgCl_2$, pH 7.4) with 30% DMSO by volume. Afterward, the sample was dialyzed against SAMA buffer (0.05 M NaOAc, 0.008 M $Mg(OAc)_2$, pH 4.6) with 30% DMSO by volume. The last dialysis of the sample was done against SAMA buffer without DMSO. Each dialysis was performed for at least 8 h at 4 °C.

VLP-Bdpy Assembly. A boron dipyrromethene dye derivative from BODIPY FL NHS was used as a model hydrophobic dye molecule to be encapsulated by BMV CPs. Prior to encapsulation, BODIPY FLS NHS dyes were reacted with glycine (Gly) to replace the NHS ester with Gly (Figure S4), thereby preventing the covalent attachment of the NHS ester to lysines on the CP (BODIPY conjugated with Gly will be referred to as Bdpy).[21] First, a solution of glycine (in TKM), Bdpy, and DMSO were mixed, covered, and incubated at room temperature for 1 h to allow for the reaction between Bdpy and glycine. To this solution, BMV CP was added at a 10 Bdpy: 1 CP ratio, and the final solution was covered and incubated at 4 °C for 1 h. The solution was adjusted such that the final protein concentration was 0.5 mg/mL. This mixture was then dialyzed against 30% DMSO EC buffer overnight, making sure to cover the assembly with foil to prevent damage to the BODIPY dyes. Then, the mixture was transferred to an aqueous solution by dialysis against 0% DMSO EC buffer.

Self-assembly of VLP-Bdpy was carried out in EC buffer (0.5 M NaCl) with 30% DMSO, after which DMSO was eliminated by dialysis against EC buffer (0.5 M NaCl) without DMSO. VLP self-assembly was carried out at 10:1 Bdpy/CP molar ratio.

Transmission Electron Microscopy (TEM) Imaging. Typically, 3 μL of VLPs was diluted with 7 μL of SAMA buffer and was placed onto a carbon-coated copper TEM grid. After 5 min, the solution was removed using Whatman filter paper 2, and the sample was stained with 2% uranyl acetate (UA) for 2 min. The excess UA was blotted off using filter paper. VLPs were imaged with a JEM-1010 TEM at 80 kV and digital images recorded with a Gatan MegaScan 794 CCD camera or JEM-1400plus TEM with a Gatan OneView CMOS digital camera. TEM images of VLPs were analyzed using ImageJ. The contour analysis of VLPs-UCNPs was performed by FFT after polar transformation and plot profile using ImageJ.

Dynamic Light Scattering Measurements. DLS characterization of VLPs was carried out with a Zetasizer Nano ZS (Malvern Instruments) and a micro quartz cell (ZEN2112). For UCNP measurements, samples were purified by centrifugation to remove aggregates and other contaminants. A solution of 1mg/mL UCNP was centrifuged at 14 000 rpm for 40 min at room temperature to sediment the UCNPs. The supernatant was discarded, and the transparent pellet was redispersed in SAMA. This solution was then centrifuged at 7 000 rpm for 1 min to remove aggregates. The supernatant was recovered and measured.

UV/Vis Absorption Measurements. UV/Vis absorption measurements were carried out using a Cary 100 Bio UV−Visible Spectrophotometer. Assembly samples were diluted 10× before measurement (dilution factors were the same when comparing different assemblies).

Linear Combination UV/Vis Fitting. IGOR Pro was used to fit absorption spectra of ECs, Bdpy in DMSO, and VLP-Bdpy to Gaussian curves. A fitting function was defined as the linear combination of the EC and Bdpy absorption spectra. The fitted VLP-Bdpy curve was then fitted using the linear combination of the EC and Bdpy spectra, and the linear combination coefficients were used to determine the ratio of CP/Bdpy.

Fluorescence Measurements. Fluorescence measurements for VLP-BDP-Gly were carried out with an Edinburgh Instruments FLS 100. The concentration of BODIPY was kept between 100 and 200 nM, with dilution factors being the same when comparing samples.

Molecular Docking Simulations. AutoDock Vina software (version 1.1.2, Scripps)[58] was employed for all docking experiments. X-ray diffraction-based crystal structure of BMV CP protein was used for this study (PDN ID 1JS9) from the RCSB Protein Data Bank (PDB). Interactions between BMV CP and DMSO and CP N-terminal region of BMV with PAA were carried out with AutoDock Vina 1.1.2 software. The coordinates of DMSO and PAA were downloaded in.sdf format from PubChem Public databases, PubChem SID 679 and SID 134214216, respectively. The files in.sdf were converted into.pdbqt format by OpenBabel software (version 2.4.1).[73] Docking was performed as described by the AutoDock Vina manual. Briefly, ions and water were removed from the PDB structures, and only the monomer of CP BMV was used (chain A). BMV CP was divided into two active site grids to study the interaction with CP, with one grid used for the N-terminal region of CP BMV. The docking between the PAA and CP only was performed in the N-terminal region of the protein. Of the nine most probable conformations, only the conformation with the highest energy in each of the regions is shown, considering that the ligand molecule only rotates or moves a distance close to its size. The energy shown in each of the images is the average of the nine most probable conformations since their affinity energies were very similar. The images and electrostatic surface of docked ligand proteins were generated with PYMOL software version 2.4.0.

https://doi.org/10.1021/acs.bioconjchem.1c00420
Bioconjugate Chem. 2021, 32, 2366−2376

■ ASSOCIATED CONTENT

Supporting Information

The Supporting Information is available free of charge at https://pubs.acs.org/doi/10.1021/acs.bioconjchem.1c00420.

TEM images of wtBMV incubated at (a) 10% (b), 20% (c) 30% DMSO for 48 h; box plots of size distributions by TEM of VLP assemblies in 30% DMSO vs core average size and providing additional samples characterization (PDF)

■ AUTHOR INFORMATION

Corresponding Authors

Bogdan Dragnea − *Department of Chemistry, Indiana University, Bloomington, Indiana 47405, United States;* orcid.org/0000-0003-0611-2006; Phone: (812)856-0087; Email: dragnea@indiana.edu

Ruben D. Cadena-Nava − *Department of Chemistry, Indiana University, Bloomington, Indiana 47405, United States;* Present Address: Centro de Nanociencias y Nanotecnología, Universidad Nacional Autónoma de México (CNyN-UNAM), Km 107 Carretera Tijuana-Ensenada, Col. Pedregal Playitas, C.P. 22860 Ensenada, Baja California, México; orcid.org/0000-0001-8428-6701; Email: rcadena74@gmail.com

Authors

Amberly Xie − *Department of Chemistry, Indiana University, Bloomington, Indiana 47405, United States*

Irina Tsvetkova − *Department of Chemistry, Indiana University, Bloomington, Indiana 47405, United States*

Yang Liu − *Department of Chemistry, Indiana University, Bloomington, Indiana 47405, United States*

Xingchen Ye − *Department of Chemistry, Indiana University, Bloomington, Indiana 47405, United States;* orcid.org/0000-0001-6851-2721

Priyadarshine Hewavitharanage − *Chemistry Department, University of Southern Indiana, Evansville, Indiana 47712, United States*

Complete contact information is available at: https://pubs.acs.org/10.1021/acs.bioconjchem.1c00420

Notes

The authors declare no competing financial interest.

■ ACKNOWLEDGMENTS

The work was supported by the Army Research Office, under Award W911NF-17-1-0329, and by the National Science Foundation, under Awards CBET 1803440 and 1808027. RDCN thanks PASPA-DGAPA-UNAM for sabbatical support. The authors gratefully acknowledge the Center for Bioanalytical Metrology (CBM), an NSF Industry-University Cooperative Research Center, for providing funding for this project under Grant NSF IIP 1916645, and Indiana University at Bloomington for access to the Electron Microscopy Center and the Nanoscience Characterization Facility.

■ REFERENCES

(1) Du, J.; Catania, C.; Bazan, G. C. Modification of Abiotic−Biotic Interfaces with Small Molecules and Nanomaterials for Improved Bioelectronics. *Chem. Mater.* **2014**, *26*, 686−697.

(2) Jans, H.; Huo, Q. Gold nanoparticle-enabled biological and chemical detection and analysis. *Chem. Soc. Rev.* **2012**, *41*, 2849−2866.

(3) Cheng, Y.; Samia, A. C.; Meyers, J. D.; Panagopoulos, I.; Fei, B.; Burda, C. Highly Efficient Drug Delivery with Gold Nanoparticle Vectors for in Vivo Photodynamic Therapy of Cancer. *J. Am. Chem. Soc.* **2008**, *130*, 10643−10647.

(4) Stuchinskaya, T.; Moreno, M.; Cook, M. J.; Edwards, D. R.; Russell, D. A. Targeted photodynamic therapy of breast cancer cells using antibody−phthalocyanine−gold nanoparticle conjugates. *Photochem. Photobiol. Sci.* **2011**, *10*, 822−831.

(5) Kumar, B.; Malhotra, K.; Fuku, R.; Van Houten, J.; Qu, G. Y.; Piunno, P. A. E.; Krull, U. J. Recent trends in the developments of analytical probes based on lanthanide-doped upconversion nanoparticles. *TrAC, Trends Anal. Chem.* **2021**, *139*, No. 116256.

(6) Esipova, T. V.; Ye, X.; Collins, J. E.; Sakadžić, S.; Mandeville, E. T.; Murray, C. B.; Vinogradov, S. A. Dendritic upconverting nanoparticles enable in vivo multiphoton microscopy with low-power continuous wave sources. *Proc. Natl. Acad. Sci. U.S.A.* **2012**, *109*, 20826.

(7) Wu, Y.; Xu, J.; Poh, E. T.; Liang, L.; Liu, H.; Yang, J. K. W.; Qiu, C.-W.; Vallée, R. A. L.; Liu, X. Upconversion superburst with sub-2 μs lifetime. *Nat. Nanotechnol.* **2019**, *14*, 1110−1115.

(8) Prigozhin, M. B.; Maurer, P. C.; Courtis, A. M.; Liu, N.; Wisser, M. D.; Siefe, C.; Tian, B.; Chan, E.; Song, G.; Fischer, S.; et al. Bright sub-20-nm cathodoluminescent nanoprobes for electron microscopy. *Nat. Nanotechnol.* **2019**, *14*, 420−425.

(9) Singh, R.; Dumlupinar, G.; Andersson-Engels, S.; Melgar, S. Emerging applications of upconverting nanoparticles in intestinal infection and colorectal cancer. *Int. J. Nanomed.* **2019**, *14*, 1027−1038.

(10) Shang, Y.; Hao, S.; Yang, C.; Chen, G. Enhancing Solar Cell Efficiency Using Photon Upconversion Materials. *Nanomaterials* **2015**, *5*, 1782−1809.

(11) Wang, M.; Abbineni, G.; Clevenger, A.; Mao, C.; Xu, S. Upconversion nanoparticles: synthesis, surface modification and biological applications. *Nanomedicine* **2011**, *7*, 710−729.

(12) Phan, H. T.; Haes, A. J. What Does Nanoparticle Stability Mean? *J. Phys. Chem. C* **2019**, *123*, 16495−16507.

(13) Dick, F. D. Solvent neurotoxicity. *Occup. Environ. Med.* **2006**, *63*, 221.

(14) Yu, Z. W.; Quinn, P. J. Dimethyl sulphoxide: A review of its applications in cell biology. *Biosci. Rep.* **1994**, *14*, 259−281.

(15) LeBel, R. G.; Goring, D. A. I. Density, Viscosity, Refractive Index, and Hygroscopicity of Mixtures of Water and Dimethyl Sulfoxide. *J. Chem. Eng. Data* **1962**, *7*, 100−101.

(16) Oh, K.-I.; You, X.; Flanagan, J. C.; Baiz, C. R. Liquid−Liquid Phase Separation Produces Fast H-Bond Dynamics in DMSO−Water Mixtures. *J. Phys. Chem. Lett.* **2020**, *11*, 1903−1908.

(17) Berz, D.; McCormack, E. M.; Winer, E. S.; Colvin, G. A.; Quesenberry, P. J. Cryopreservation of hematopoietic stem cells. *Am. J. Hematol.* **2007**, *82*, 463−472.

(18) Meneghel, J.; Kilbride, P.; Morris, J. G.; Fonseca, F. Physical events occurring during the cryopreservation of immortalized human T cells. *PLoS One* **2019**, *14*, No. e0217304.

(19) Hochstrat, E.; Müller, M.; Frank, A.; Michel, P.; Hansen, U.; Raschke, M. J.; Kronenberg, D.; Stange, R. Cryopreservation of tendon tissue using dimethyl sulfoxide combines conserved cell vitality with maintained biomechanical features. *PLoS One* **2019**, *14*, No. e0215595.

(20) Shangguan, L.; Chen, Q.; Shi, B.; Huang, F. Enhancing the solubility and bioactivity of anticancer drug tamoxifen by water-soluble pillar[6]arene-based host−guest complexation. *Chem. Commun.* **2017**, *53*, 9749−9752.

(21) Dorh, N.; Zhu, S.; Dhungana, K. B.; Pati, R.; Luo, F.-T.; Liu, H.; Tiwari, A. BODIPY-Based Fluorescent Probes for Sensing Protein Surface-Hydrophobicity. *Sci. Rep.* **2015**, *5*, No. 18337.

(22) Cao, M.; Yu, L.; Zhang, P.; Xiong, H.; Jin, Y.; Lu, Y.; Wang, L.-Q. Soft-binding ligand-capped fluorescent CdSe/ZnS quantum dots

for the facile labeling of polysaccharide-based self-assemblies. *Colloids Surf., B* **2013**, *109*, 154−160.
(23) Pramanik, C.; Gissinger, J. R.; Kumar, S.; Heinz, H. Carbon Nanotube Dispersion in Solvents and Polymer Solutions: Mechanisms, Assembly, and Preferences. *ACS Nano* **2017**, *11*, 12805−12816.
(24) Ju-Nam, Y.; Abdussalam-Mohammed, W.; Ojeda, J. J. Highly stable noble metal nanoparticles dispersible in biocompatible solvents: synthesis of cationic phosphonium gold nanoparticles in water and DMSO. *Faraday Discuss.* **2016**, *186*, 77−93.
(25) Luzar, A.; Chandler, D. Structure and hydrogen bond dynamics of water−dimethyl sulfoxide mixtures by computer simulations. *J. Chem. Phys.* **1993**, *98*, 8160−8173.
(26) Arakawa, T.; Kita, Y.; Timasheff, S. N. Protein precipitation and denaturation by dimethyl sulfoxide. *Biophys. Chem.* **2007**, *131*, 62−70.
(27) Chan, D. S. H.; Kavanagh, M. E.; McLean, K. J.; Munro, A. W.; Matak-Vinković, D.; Coyne, A. G.; Abell, C. Effect of DMSO on Protein Structure and Interactions Assessed by Collision-Induced Dissociation and Unfolding. *Anal. Chem.* **2017**, *89*, 9976−9983.
(28) Hanslick, J. L.; Lau, K.; Noguchi, K. K.; Olney, J. W.; Zorumski, C. F.; Mennerick, S.; Farber, N. B. Dimethyl sulfoxide (DMSO) produces widespread apoptosis in the developing central nervous system. *Neurobiol. Dis.* **2009**, *34*, 1−10.
(29) Galvao, J.; Davis, B.; Tilley, M.; Normando, E.; Duchen, M. R.; Cordeiro, M. F. Unexpected low-dose toxicity of the universal solvent DMSO. *FASEB J.* **2014**, *28*, 1317−1330.
(30) Soto, C. M.; Blum, A. S.; Vora, G. J.; Lebedev, N.; Meador, C. E.; Won, A. P.; Chatterji, A.; Johnson, J. E.; Ratna, B. R. Fluorescent Signal Amplification of Carbocyanine Dyes Using Engineered Viral Nanoparticles. *J. Am. Chem. Soc.* **2006**, *128*, 5184−5189.
(31) Steinmetz, N. F. Viral nanoparticles as platforms for next-generation therapeutics and imaging devices. *Nanomedicine* **2010**, *6*, 634−641.
(32) Qazi, S.; Liepold, L. O.; Abedin, M. J.; Johnson, B.; Prevelige, P.; Frank, J. A.; Douglas, T. P22 Viral Capsids as Nanocomposite High-Relaxivity MRI Contrast Agents. *Mol. Pharmaceutics* **2013**, *10*, 11−17.
(33) Steele, J. F. C.; Peyret, H.; Saunders, K.; Castells-Graells, R.; Marsian, J.; Meshcheriakova, Y.; Lomonossoff, G. P. Synthetic plant virology for nanobiotechnology and nanomedicine. *Wiley Interdiscip. Rev.: Nanomed. Nanobiotechnol.* **2017**, *9*, No. e1447.
(34) Biddlecome, A.; Habte, H. H.; McGrath, K. M.; Sambanthamoorthy, S.; Wurm, M.; Sykora, M. M.; Knobler, C. M.; Lorenz, I. C.; Lasaro, M.; Elbers, K.; Gelbart, W. M. Delivery of self-amplifying RNA vaccines in in vitro reconstituted virus-like particles. *PLoS One* **2019**, *14*, No. e0215031.
(35) Schwarz, B.; Douglas, T. Development of virus-like particles for diagnostic and prophylactic biomedical applications. *Wiley Interdiscip. Rev.: Nanomed. Nanobiotechnol.* **2015**, *7*, 722−735.
(36) Vieweger, S. E.; Tsvetkova, I. B.; Dragnea, B. G. In Vitro Assembly of Virus-Derived Designer Shells Around Inorganic Nanoparticles. In *Methods in Molecular Biology*, Springer Nature, 2018; Vol. *1776*, pp 279−294.
(37) Chan, J. C.; Gadebusch, H. H. Virucidal properties of dimethyl sulfoxide. *Appl. Microbiol.* **1968**, *16*, 1625−1626.
(38) Wilson, T. M. A.; Lomonossoff, G. P.; Glover, J. F. Dimethyl Sulphoxide (DMSO) Disassembles Tobacco Mosaic Virus Predominantly from the 5′-end of the Viral RNA. *J. Gen. Virol.* **1981**, *53*, 225−234.
(39) Hull, R. Purification and Composition of Plant Viruses. In *Matthews' Plant Virology*, 4th ed.; Hull, R., Ed.; Academic Press:London, 2002; pp 75−107.
(40) Chatterji, A.; Ochoa, W.; Shamieh, L.; Salakian, S. P.; Wong, S. M.; Clinton, G.; Ghosh, P.; Lin, T.; Johnson, J. E. Chemical Conjugation of Heterologous Proteins on the Surface of Cowpea Mosaic Virus. *Bioconjugate Chem.* **2004**, *15*, 807−813.
(41) Wang, Q.; Kaltgrad, E.; Lin, T.; Johnson, J. E.; Finn, M. G. Natural supramolecular building blocks. Wild-type cowpea mosaic virus. *Chem. Biol.* **2002**, *9*, 805−811.
(42) Bruckman, M. A.; Steinmetz, N. F. Chemical modification of the inner and outer surfaces of Tobacco Mosaic Virus (TMV). *Methods Mol. Biol.* **2014**, *1108*, 173−185.
(43) Yildiz, I.; Tsvetkova, I.; Wen, A. M.; Shukla, S.; Masarapu, M. H.; Dragnea, B.; Steinmetz, N. F. Engineering of Brome mosaic virus for biomedical applications. *RSC Adv.* **2012**, *2*, 3670−3677.
(44) Wen, A. M.; Lee, K. L.; Yildiz, I.; Bruckman, M. A.; Shukla, S.; Steinmetz, N. F. Viral nanoparticles for in vivo tumor imaging. *J. Visualized Exp.* **2012**, No. e4352.
(45) Cao, T.; Yang, Y.; Gao, Y.; Zhou, J.; Li, Z.; Li, F. High-quality water-soluble and surface-functionalized upconversion nanocrystals as luminescent probes for bioimaging. *Biomaterials* **2011**, *32*, 2959−2968.
(46) Wang, Z.; Zhang, T.; Pi, L.; Xiang, H.; Dong, P.; Lu, C.; Jin, T. Large-scale one-pot synthesis of water-soluble and biocompatible upconversion nanoparticles for dual-modal imaging. *Colloids Surf., B* **2021**, *198*, No. 111480.
(47) Cui, Y.; Chen, B.; Qian, G. Lanthanide metal-organic frameworks for luminescent sensing and light-emitting applications. *Coord. Chem. Rev.* **2014**, *273-274*, 76−86.
(48) Wróbel, R.; Chmurzyński, L. Potentiometric pKa determination of standard substances in binary solvent systems. *Anal. Chim. Acta* **2000**, *405*, 303−308.
(49) Pfeiffer, P.; Hirth, L. Aggregation states of brome mosaic virus protein. *Virology* **1974**, *61*, 160−167.
(50) Cuillel, M.; Berthet-Colominas, C.; Timmins, P. A.; Zulauf, M. Reassembly of brome mosaic virus from dissociated virus. *Eur. Biophys. J.* **1987**, *15*, 169−176.
(51) Delalande, L.; Tsvetkova, I. B.; Zeng, C.; Bond, K.; Jarrold, M. F.; Dragnea, B. Catching a virus in a molecular net. *Nanoscale* **2016**, *8*, 16221−16228.
(52) Cuillel, M.; Zulauf, M.; Jacrot, B. Self-assembly of brome mosaic virus protein into capsids: Initial and final states of aggregation. *J. Mol. Biol.* **1983**, *164*, 589−603.
(53) Bharmoria, P.; Gupta, H.; Mohandas, V. P.; Ghosh, P. K.; Kumar, A. Temperature Invariance of NaCl Solubility in Water: Inferences from Salt−Water Cluster Behavior of NaCl, KCl, and NH4Cl. *J. Phys. Chem. B* **2012**, *116*, 11712−11719.
(54) Long, B. Experimental Studies and Thermodynamic Modeling of the Solubilities of Potassium Nitrate, Potassium Chloride, Potassium Bromide, and Sodium Chloride in Dimethyl Sulfoxide. *Ind. Eng. Chem. Res.* **2011**, *50*, 7019−7026.
(55) Pfeiffer, P.; Herzog, M.; Hirth, L. RNA viruses: stabilization of brome mosaic virus. *Philos. Trans. R. Soc., B* **1976**, *276*, 99−107.
(56) Mancera, R. L.; Chalaris, M.; Samios, J. The concentration effect on the 'hydrophobic' and 'hydrophilic' behaviour around DMSO in dilute aqueous DMSO solutions. A computer simulation study. *J. Mol. Liq.* **2004**, *110*, 147−153.
(57) Zulauf, M. Swelling of brome mosaic virus as studied by intensity fluctuation spectroscopy. *J. Mol. Biol.* **1977**, *114*, 259−266.
(58) Trott, O.; Olson, A. J. AutoDock Vina: improving the speed and accuracy of docking with a new scoring function, efficient optimization, and multithreading. *J. Comput. Chem.* **2010**, *31*, 455−461.
(59) Tunçer, S.; Gurbanov, R.; Sheraj, I.; Solel, E.; Esenturk, O.; Banerjee, S. Low dose dimethyl sulfoxide driven gross molecular changes have the potential to interfere with various cellular processes. *Sci. Rep.* **2018**, *8*, No. 14828.
(60) Roy, S.; Bagchi, B. Comparative Study of Protein Unfolding in Aqueous Urea and Dimethyl Sulfoxide Solutions: Surface Polarity, Solvent Specificity, and Sequence of Secondary Structure Melting. *J. Phys. Chem. B* **2014**, *118*, 5691−5697.
(61) Burke, A.; Chevreuil, M.; Paris, A.; de La Grange, V.; Goldmann, C.; Pérez, J.; Constantin, D.; Tresset, G. Nanoparticle-Templated Self-Assembly of Viral Capsids Probed by Time-Resolved Absorbance Spectroscopy and X-Ray Scattering. *Phys. Rev. Appl.* **2018**, *10*, No. 054065.
(62) Nuñez-Rivera, A.; Fournier, P. G. J.; Arellano, D. L.; Rodriguez-Hernandez, A. G.; Vazquez-Duhalt, R.; Cadena-Nava, R. D. Brome

https://doi.org/10.1021/acs.bioconjchem.1c00420
Bioconjugate Chem. 2021, 32, 2366−2376

mosaic virus-like particles as siRNA nanocarriers for biomedical purposes. *Beilstein J. Nanotechnol.* **2020**, *11*, 372−382.
(63) Ghosh, S.; Banerjee, M. A smart viral vector for targeted delivery of hydrophobic drugs. *Sci. Rep.* **2021**, *11*, No. 7030.
(64) Bourne, C.; Lee, S.; Venkataiah, B.; Lee, A.; Korba, B.; Finn, M. G.; Zlotnick, A. Small-molecule effectors of hepatitis B virus capsid assembly give insight into virus life cycle. *J. Virol.* **2008**, *82*, 10262−10270.
(65) Tan, Z.; Pionek, K.; Unchwaniwala, N.; Maguire, M. L.; Loeb, D. D.; Zlotnick, A. The interface between hepatitis B virus capsid proteins affects self-assembly, pregenomic RNA packaging, and reverse transcription. *J. Virol.* **2015**, *89*, 3275−3284.
(66) Das, N. C.; Warren, G. T.; Kao, C. C.; Dragnea, B. G.; Ni, P.; Sokol, P. E. Small Angle Scattering Study of the Structure and Organization of RNAs and Protein of Brome Mosaic Virus (BMV) Capsid Protein. *Phys. Procedia* **2014**, *60*, 101−109.
(67) Lucas, R. W.; Larson, S. B.; McPherson, A. The Crystallographic Structure of Brome Mosaic Virus. *J. Mol. Biol.* **2002**, *317* (1), 95−108.
(68) Slot, J. W.; Geuze, H. J. A new method of preparing gold probes for multiple-labeling cytochemistry. *Eur. J. Cell Biol.* **1985**, *38*, 87−93.
(69) Ye, X.; Collins, J. E.; Kang, Y.; Chen, J.; Chen, D. T. N.; Yodh, A. G.; Murray, C. B. Morphologically controlled synthesis of colloidal upconversion nanophosphors and their shape-directed self-assembly. *Proc. Natl. Acad. Sci. U.S.A.* **2010**, *107*, 22430.
(70) Dong, A.; Ye, X.; Chen, J.; Kang, Y.; Gordon, T.; Kikkawa, J. M.; Murray, C. B. A Generalized Ligand-Exchange Strategy Enabling Sequential Surface Functionalization of Colloidal Nanocrystals. *J. Am. Chem. Soc.* **2011**, *133*, 998−1006.
(71) Bancroft, J. B. The Self-Assembly Of Spherical Plant Viruses. In *Advances in Virus Research*; Smith, K. M.; Lauffer, M. A.; Bang, F. B., Eds.; Academic Press, 1970; Vol. *16*, pp 99−134.
(72) Mackenzie, L. E.; Goode, J. A.; Vakurov, A.; Nampi, P. P.; Saha, S.; Jose, G.; Millner, P. A. The theoretical molecular weight of NaYF4:RE upconversion nanoparticles. *Sci. Rep.* **2018**, *8*, No. 1106.
(73) O'Boyle, N. M.; Banck, M.; James, C. A.; Morley, C.; Vandermeersch, T.; Hutchison, G. R. Open Babel: An open chemical toolbox. *J. Cheminf.* **2011**, *3*, No. 33.

https://doi.org/10.1021/acs.bioconjchem.1c00420
Bioconjugate Chem. 2021, 32, 2366−2376